VOLUME 117, NUMBER 30
AUGUST 2, 1995

JOURNAL OF THE AMERICAN CHEMICAL SOCIETY

Selective Nucleation and Growth of an Organic Polymorph by Ledge-Directed Epitaxy on a Molecular Crystal Substrate

Salvatore J. Bonafede and Michael D. Ward*

Contribution from the Department of Chemical Engineering and Materials Science, University of Minnesota, Amundson Hall, 421 Washington Avenue SE, Minneapolis, Minnesota 55455

Received March 29, 1995[⊗]

Abstract: Selective growth of a thermodynamically less preferred polymorph of the salt $(DMTC^+)(TMO^-)\cdot CHCl_3$ (DMTC = 3,3′-dimethylthiacarbocyanine; TMO = 3,3′,5,5′-tetramethyltrimethine oxonol) has been achieved from $CHCl_3$ solutions by nucleation on single-crystal succinic acid (SA) substrates. This process occurs by a ledge-directed epitaxy (LDE) mechanism in which the dihedral angle between two close-packed planes of a substrate ledge site matches that of two close-packed planes of a prenucleation aggregate corresponding to the observed polymorph. The observed orientation of $(DMTC^+)(TMO^-)\cdot CHCl_3$ is consistent with interaction of the close-packed (010) and (014) planes of its aggregate with succinic acid $(0\bar{1}0)$ and $(1\bar{1}\bar{1})$ planes that define ledges along the $[10\bar{1}]$ direction of the substrate. These ledge sites are produced readily by cleavage of SA single crystals. The identity of the polymorph and its orientation are confirmed by visible spectroscopy, crystal morphology, and atomic force microscopy. While LDE allows for two possible orientations of $(DMTC^+)(TMO^-)\cdot CHCl_3$, the orientation observed is that in which the lattice mismatch along the interface is minimized. These observations illustrate that crystallization processes based on LDE may be valuable for selective growth of polymorphs.

Introduction

Molecular crystals are composed of discrete molecules held together in the solid state by weak intermolecular forces. The growth of a molecular crystal can be described as a stepwise self-assembly process in which molecules initially form a prenucleation aggregate which evolves into a stable crystal nucleus and, ultimately, a macroscopic crystal. It is generally accepted that heterogeneous nucleation on surfaces is energetically more favorable than homogeneous nucleation.[1,2] This principle has been combined with a molecular level view of nucleation to achieve a systematic design of molecular interfaces which direct the crystallization process. For example, the influence of interface structure on nucleation rates and crystal orientation has been demonstrated for Langmuir[3] and organosulfur[4,5] monolayers. These strategies rely upon a model in which the prenucleation aggregate must resemble the mature crystal structure at some point during the crystallization process.[6] Consequently, the interface is designed to resemble a particular crystal plane of the desired material. Crystallization of planar aromatic molecules[7-9] and long-chain hydrocarbons[10,11] on ordered solid substrates has illustrated the role of epitaxy

* Author to whom correspondence should be addressed.
⊗ Abstract published in *Advance ACS Abstracts*, July 1, 1995.

(1) Chalmers, B. *Principles of Solidification*; Robert E. Krieger Publishing Co.: Huntington, NY, 1964.
(2) Chakraverty, B. K. In *Crystal Growth: An Introduction*; Hartman, P., Ed.; North Holland Publishing Co.: Amsterdam, 1973.
(3) (a) Heywood, B. R.; Mann, S. *J. Am. Chem. Soc.* **1992**, *114*, 4681. (b) Popovitz-Biro, R.; Lahav, M.; Leiserowitz, L. *J. Am. Chem. Soc.* **1991**, *113*, 8943. (c) Landau, E. M.; Wolf, S. G.; Levanon, M.; Leiserowitz, L.; Lahav, M.; Sagiv, J. *J. Am. Chem. Soc.* **1989**, *111*, 1436.
(4) Campbell, A. A.; Fryxell, G. E.; Graff, G. L.; Reike, P. C.; Tarasevich, B. *J. Scanning Microsc.* **1993**, *7*, 423.
(5) Frostman, L. M.; Bader, M. M.; Ward, M. D. *Langmuir* **1994**, *10*, 576.
(6) Addadi, L.; Berkovitch-Yellin, Z.; Weissbuch, I.; van Mil, J.; Shimon, L. J. W.; Lahav, M.; Leiserowitz, L. *Angew. Chem., Int. Ed. Engl.* **1985**, *24*, 466.
(7) Zimmermann, U.; Schnitzler, G.; Karl, N.; Umbach, E. *Thin Solid Films* **1989**, *175*, 85.

0002-7863/95/1517-7853$09.00/0

between the substrate and growing crystal. Recent scanning tunneling and atomic force microscopy studies have revealed ordered arrangements of molecules and liquid crystals on solid substrates, reflecting interfacial interactions that may be relevant to heterogeneous nucleation.[12-15] Substrate topography also can play an important role in crystallization, with nucleation occurring readily in substrate cracks where interfacial contact between the substrate and the nutrient-rich phase is increased.[1] Ice crystallization in microcrevices of an amino acid single-crystal substrate has been reported recently.[16]

Many commercial crystallization processes aim to control crystal characteristics such as morphology, size, and polymorphism, as these characteristics can influence solid flow characteristics, solubility, processibility, mechanical properties, bioavailability and ease of delivery of pharmaceutics,[17,18] and effectiveness of dyes in photographic applications. Organic crystals are prone to forming polymorphs owing to the relatively weak and nondirectional intermolecular interactions in the solid state. However, for a given composition (at a given temperature and pressure), only a single phase can lie at the thermodynamic minimum. Barring solid-state transformations, the formation of polymorphs therefore is a consequence of different activation energies for nucleation of the different crystal forms. Recent studies have demonstrated that substrates upon which nucleation occurs play an important role in polymorph selectivity. Selectivity for different anthranilic acid polymorphs was achieved by "chemotaxy", which involves specific chemical interaction between nuclei and functionalities exposed at silane-modified glass surfaces.[19] Selective nucleation of β-(bis(ethylenedithiolo)tetrathiafulvalene)$_2$ triodide on highly oriented pyrolytic graphite was achieved by a specific quasiepitaxial commensurism between the ordered substrate and nuclei corresponding to this polymorph.[20]

It was demonstrated recently in our laboratory that crystallographically well-defined ledges (a ledge corresponds to the intersection of a terrace plane and a step plane on a crystal surface) can serve as nucleation sites for organic crystals through a mechanism described as "ledge-directed epitaxy" (LDE). The LDE principle relies on a geometric match, based on interplanar dihedral angles, between the two close-packed planes of the ledge site and two close-packed planes of a prenucleation aggregate corresponding to the growing phase.[21] These observations prompted us to examine whether the LDE concept could be extended to the selective nucleation of organic polymorphs by tailoring the substrate ledge geometry to match that of an aggregate corresponding to a desired polymorph.

We report herein the selective nucleation and growth of a polymorph of the salt (DMTC$^+$)(TMO$^-$)$\cdot$CHCl$_3$ (DMTC = 3,3′-dimethylthiacarbocyanine; TMO = 3,3′,5,5′-tetramethyltrimethine oxonol), which is driven by LDE on a succinic acid (SA) substrate. Fourteen polymorphs and pseudopolymorphs of

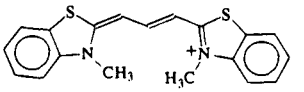

DMTC

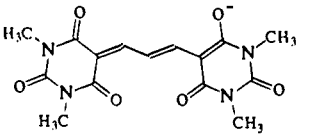

TMO

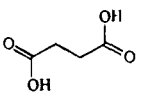

SA

DMTC$^+$−TMO$^-$ salts have been identified,[22] forming either directly during crystallization or by thermally driven solid-state phase transitions. These dye salts were particularly attractive for examining the influence of LDE on polymorph selectivity because their different colors allowed for easy identification of the polymorphs. Our studies have revealed that, whereas crystallizations from chloroform afforded three polymorphs in varying proportions, nucleation of a single, less thermodynamically preferred polymorph was observed at exposed $[10\bar{1}]_{SA}$ ledge sites of freshly cleaved SA crystals. The identity and orientation of the observed crystals with respect to the SA substrate were consistent with nucleation driven by LDE. Polymorph selectivity was also achieved when crystallization was performed in the presence of freshly ground microscopic seeds of SA. These results suggest that the LDE principle, which is based on molecular level concepts, can be used to control polymorphism in crystallization processes.

Experimental Section

Succinic acid (Fluka), DMTC and TMO (Rochelle Crystal Co.), and chloroform (Fisher) were used without further purification. Substrate crystals of β-succinic acid were grown by slow evaporation of an aqueous solution prepared with deionized 18 MΩ water, giving diamond-shaped platelike crystals with dimensions of approximately 5 × 3 mm. The SA crystals used for crystal growth studies were cleaved with a sharp razor blade along the $[001]_{SA}$ direction, affording large $\{0\bar{1}0\}_{SA}$ faces.

Crystallization studies were peformed by placing SA substrate crystals in petri dishes so that the freshly cleaved $\{0\bar{1}0\}_{SA}$ surfaces were facing toward air, followed by addition of 10 mL of a CHCl$_3$ solution containing 7.5 × 10^{-5} M DMTC and TMO. The solutions were covered and allowed to stand for 24−36 h, after which (DMTC$^+$)(TMO$^-$)$\cdot$CHCl$_3$ crystals were evident on the SA substrates from optical microscopy. Longer crystallization times were avoided to ensure against dissolution of the substrate crystals.

Optical micrographs were taken with an Olympus SZH microscope equipped with a Polaroid camera and a JVC color video camera. UV−vis spectroscopy was performed on a Hewlett Packard HP8452 diode array spectrometer. Samples were prepared in a Nujol mull with crystals which had been removed from the SA substrate. Atomic force microscopy (AFM) was performed with a Digital Instruments Nanoscope III equipped with a scanner having a maximum scan range of 15 × 15 × 4.4 μm^3 and a Si_3N_4 tip with a force constant of 0.06 N/m. The AFM was calibrated against highly oriented pyrolytic graphite standards. All AFM images were taken in air at room temperature, directly on crystals attached to the SA substrates.

Concept of Polymorph Selectivity by Ledge-Directed Epitaxy. A conceptual framework based on Gibbs−Volmer theory of homoge-

(8) Yanagi, H.; Takemoto, K.; Hayashi, S.; Ashida, M. *J. Cryst. Growth* **1990**, *99*, 1038.
(9) Hayashi, S.; Ikuno, H.; Yanagi, H; Ashida, M. *J. Cryst. Growth* **1992**, *123*, 35.
(10) Kawaguchi, A.; Okihara, T.; Ohara, M.; Tsuji, M.; Katayama, K. *J. Cryst. Growth* **1989**, *94*, 857.
(11) Kawaguchi, A.; Okihara, T.; Katayama, K. *J. Cryst. Growth* **1990**, *99*, 1028.
(12) Foster, J. S.; Frommer, J. E. *Nature* **1988**, *333*, 542.
(13) Frommer, J. *Angew. Chem., Int. Ed. Engl.* **1992**, *31*, 1298.
(14) Patrick, D. L.; Cee, V. J.; Beebe, T. P., Jr. *Science* **1994**, *265*, 231.
(15) Cai, H.; Hillier, A. C.; Franklin, K. R.; Nunn, C. C.; Ward, M. D. *Science* **1994**, *266*, 1551.
(16) Gavish, M.; Wang, J.-L.; Einstein, M.; Lahav, M.; Leiserowitz, L. *Science* **1992**, *256*, 815.
(17) Byrn, S. R. *Solid-State Chemistry of Drugs*; Acedemic Press, Inc.: New York, 1982.
(18) Carstensen, J. T. *Pharmaceutics of Solids and Solid Dosage Forms*; John Wiley and Sons: New York, 1977.
(19) Carter, P. W.; Ward, M. D. *J. Am. Chem. Soc.* **1994**, *116*, 769.
(20) Hillier, A. C.; Maxson, J. B.; Ward, M. D. *Chem. Mater.* **1994**, *6*, 2222.
(21) Carter, P. W.; Ward, M. D. *J. Am. Chem. Soc.* **1993**, *115*, 11521.
(22) Etter, M. C.; Kress, R. B.; Bernstein, J.; Cash, D. J. *J. Am. Chem. Soc.* **1984**, *106*, 6921.

neous nucleation describes a free energy change, $\Delta G(r)$, which depends upon the size of the nucleus. This size dependence is a consequence of the surface free energy ($4\pi r^2\gamma$) and the volume free energy ($^4/_3\pi r^3\Delta G_v$) associated with the growing nucleus (eq 1). The term γ refers to the specific surface energy associated with the phase boundary between the nucleus and the nutrient medium. The surface free energy term is inherently unfavorable owing to this phase boundary, whereas the volume free energy favors nucleus formation owing to intermolecular bonding interactions. These two competing factors conspire to produce a maximum in $\Delta G(r)$ at which a critical radius ($r_{c,hom}$) is achieved (eq 2). At this point, the nucleus has an equal chance of redissolving or growing into a mature crystal. The free energy change at $r_{c,hom}$, which is tantamount to an activation barrier for nucleation, is dependent upon γ and ΔG_v (eq 3).[2,23]

$$\Delta G(r) = 4\pi r^2\gamma + \frac{4}{3}\pi r^3\Delta G_v \tag{1}$$

$$r_{c,hom} = -\frac{2\gamma}{\Delta G_v} \tag{2}$$

$$\Delta G^*_{hom} = \frac{16\pi}{3}\left(\frac{\gamma^3}{\Delta G_v^2}\right) \tag{3}$$

Heterogeneous nucleation on substrates is generally considered to be energetically less demanding than homogeneous nucleation due to lowering of the surface energy of the nucleus and the substrate upon interfacial contact. Heterogeneous nucleation can be described by expressions for a critical radius and activation barrier (eqs 4 and 5)

$$r_{c,het} = -\frac{2\gamma}{\Delta G_v} \tag{4}$$

$$\Delta G^*_{het} = \frac{16\pi}{3}\left(\frac{\gamma^3}{\Delta G^2}\right)f(\theta) \tag{5}$$

which are similar to those for homogeneous nucleation. While eqs 2 and 4 appear identical, fewer molecules are contained within the volume described by the critical radius $r_{c,het}$ because of substrate wetting by the nucleus. In this case, the activation energy is modified by a function $f(\theta)$, which describes the interaction of the nucleus with the substrate surface in terms of a classical wetting contact angle θ (eq 6).

$$f(\theta) = \frac{1}{4}(2 + \cos\theta)(1 - \cos\theta)^2 \tag{6}$$

Inspection of eq 6 reveals that $f(\theta) < 1$ for values of $\theta < 90°$ (that is, favorable wetting). Consequently, $\Delta G^*_{het} < \Delta G^*_{hom}$ under these conditions.

The wetting analogy of heterogeneous nucleation allows this process to be described conveniently in terms of the accompanying change in total surface free energy, $\Delta\gamma_{het}$ (eq 7), where γ_{32}, γ_{21}, and γ_{31} are the

$$\Delta\gamma_{het} = \gamma_{32}S_{32} + (\gamma_{21} - \gamma_{31})S_{21} \tag{7}$$

individual interfacial energies between the nutrient phase and aggregate, the aggregate and substrate, and the nutrient phase and substrate, respectively.[24] The terms S_{32} and S_{21} are the interfacial contact areas of the nutrient phase and aggregate and of the aggregate and substrate, respectively. It can be shown that larger values of θ correspond to smaller values of S_{21} for a given nucleus volume.

It is evident from these relationships that under conditions where aggregate−substrate interactions are favorable, that is, negative values of $(\gamma_{21} - \gamma_{31})$, increasing S_{21} lowers the activation energy for nucleation. The value of S_{21} for nucleation on a single substrate plane is defined by a single interface. However, if a nucleus of identical volume is able to contact two substrate planes, such as the terrace and step planes at a crystal substrate ledge site, S_{21} will be larger and the activation energy for nucleation will be lowered (for simplicity, we assume here that γ_{21} and γ_{31} are identical for both planes). This condition, which is related to conventional models of crystal growth where attachment of atoms or molecules occurs preferentially at step sites,[25,26] is the basis for nucleation driven by ledge-directed epitaxy (LDE) on surfaces of single crystals.[21]

Entropic considerations alone dictate that a crystal surface will have defects under ambient conditions, most likely in the form of steps which intersect terraces of larger area. The intersection of the step and terrace planes defines a ledge, $[uvw]_{sub}$, having a crystallographically well-defined dihedral angle, θ_{sub} (Figure 1). Step and terrace planes comprising the ledge will tend to be close-packed and dispersive in nature. It is commonly accepted that, in the early stages of crystallization prior to nucleation, a prenucleation aggregate forms that possesses a supramolecular motif resembling the solid-state structure of the mature crystal. According to the LDE principle, the free energy of the prenucleation aggregate, and the corresponding activation energy for nucleation, is lowered by interaction with the substrate ledge site if (1) its contacting planes are dispersive in nature so that interfacial interactions are attractive and repulsive interactions are minimized, (2) its contacting planes are close-packed surfaces in order to maximize interfacial interactions, and (3) the angle between the contacting aggregate planes, θ_{agg}, has approximately the same value as θ_{sub}. Appropriate aggregate planes can be deduced from inspection of the crystal structure. If two planes in the crystal structure have a dihedral angle similar to that of the substrate ledge, the condition $\theta_{agg} \approx \theta_{sub}$ will lead to a larger S_{21} term and, consequently, to enhanced interfacial stabilization of the aggregate. Conversely, if θ_{agg} is grossly different than θ_{sub}, S_{21} will be limited to a single interface and the activation barrier for nucleation will be larger than that for interaction at two interfaces at the ledge. Indeed, our previous studies demonstrated that growth occurred only on ledges when the LDE conditions were fulfilled, illustrating the lower activation energy on ledges compared to single terrace planes.[21] These studies also demonstrated that the nondirectional nature of dispersive interactions at the LDE interfaces favored growth orientation dictated solely by the geometric match between the ledge and the aggregate.

Well-defined substrate ledge sites will be favored along crystallographic directions containing strong intermolecular bonding, such as hydrogen-bonding or $\pi-\pi$ charge-transfer interactions. This condition exists in organic diacids having the general formula $HOOC(CH_2)_n$-COOH ($n = 0-16$), as these compounds possess one-dimensional chains that form as a consequence of hydrogen bonding between carboxylic acid groups. For example, succinic acid ($n = 2$; $P2_1/c$, a = 5.519 Å, b = 8.862 Å, c = 5.101 Å, β = 91.6°)[27] can be cleaved readily parallel to the $(0\bar{1}0)_{SA}$ plane, which contains hydrogen-bonded succinic acid chains organized into $(0\bar{1}0)_{SA}$ layers held together by dispersive interactions. Cleaving produces distinct linear features when the crystals are viewed normal to the $(0\bar{1}0)_{SA}$ surfaces, which can be identified as $[10\bar{1}]_{SA}$ ledges. The SA molecules are assembled by hydrogen bonding between carboxylic acid groups into one-dimensional hydrogen-bonded chains along the $[10\bar{1}]_{SA}$ ledge. These ledges are formed by the intersection of $(0\bar{1}0)_{SA}$ terrace and $(1\bar{1}1)_{SA}$ step planes and have a crystallographically defined dihedral angle of $\theta_{sub} = 112.6°$ (the planes are assigned these indices in order to be consistent with the notation in ref 21). Both planes can be considered as low-energy, close-packed, dispersive planes. The absence of hydrogen bonding between $(0\bar{1}0)_{SA}$ layers and $(1\bar{1}1)_{SA}$ layers leads to smaller critical shear stresses for slip in these planes compared to others in the crystal and favors their formation upon cleaving. The strong hydrogen bonding along $[10\bar{1}]_{SA}$ stabilizes the $(0\bar{1}0)_{SA}$ and $(1\bar{1}1)_{SA}$ planes, thereby favoring their formation when SA crystals are cleaved while also inhibiting their reconstruction. Interestingly, organic diacids display an assortment of dihedral angles for the ledge sites defined by these hydrogen-bonded chains, ranging from 90° to 140° (for succinic acid, $\theta_{sub} = 112.6°$).

(23) Schneider, H. G.; Ruth, V.; Kormany, T. *Advances in Epitaxy and Endotaxy*; Elsevier: Amsterdam, 1990; pp 313−320.
(24) Fletcher, N. H. *J. Chem. Phys.* **1963**, *38*, 237.
(25) Tiller, W. A. *The Science of Crystallization: Microscopic Interfacial Phenomena*; Cambridge University Press: New York, 1991; pp 327−381.
(26) Bennema, P.; Gilmer, G. In *Crystal Growth: An Introduction*; Hartman, P., Ed.; North Holland: Amsterdam, The Netherlands, 1973; p 272.
(27) Leviel, J.-L.; Auvert, G.; Savariault, J.-M. *Acta Crystallogr.* **1981**, *B37*, 2185.

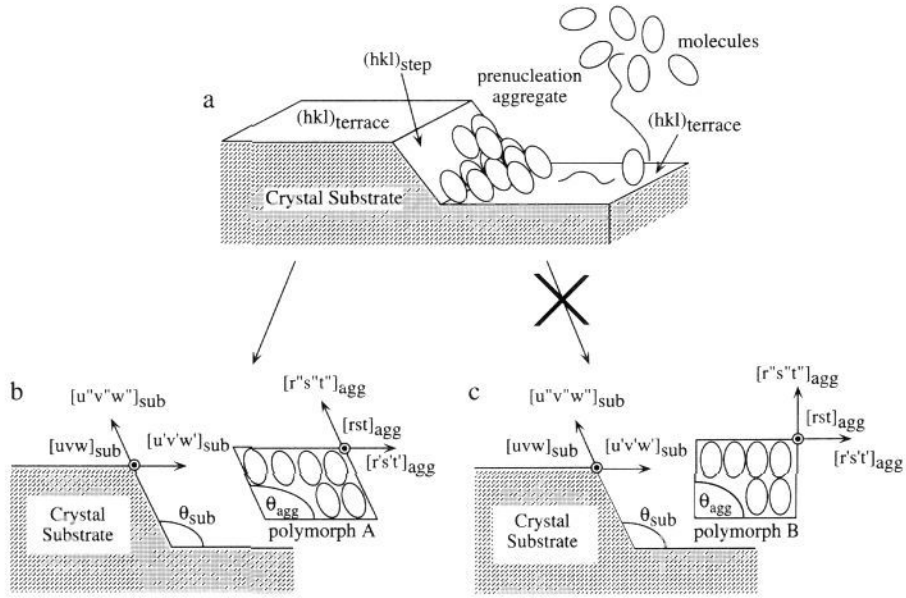

Figure 1. Schematic representation of ledge-directed epitaxy on a single-crystal substrate and the role of LDE in selective nucleation of polymorphs. The ledge site is described by a direction $[uvw]_{sub}$ and is defined by the intersection of a $(hkl)_{step}$ and a $(hkl)_{terrace}$ plane. Molecules are thought to attach preferentially to the ledge site due to enhanced stability associated with interfacial interactions with two substrate planes, instead of only one available from attachment to the terrace. In b, the dihedral angle between two low-energy planes of the aggregate (θ_{agg}) corresponding to polymorph A matches the dihedral angle of the substrate (θ_{sub}), providing interfacial contact at both planes of the ledge site. In contrast, c depicts a polymorph B, in which the dihedral angle between two low-energy planes differs substantially from that of the substrate ledge ($\theta_{agg} \neq \theta_{sub}$). The directions $[u'v'w']_{sub}$ and $[u''v''w'']_{sub}$ are contained within the step and terrace planes, respectively, and are perpendicular to the ledge direction $[uvw]_{sub}$. The direction $[uvw]_{sub}$ is normal to the plane of the paper. The terms $[rst]_{agg}$, $[r's't']_{agg}$, and $[r''s''t'']_{agg}$ are the directions along the faces of the prenucleation aggregate. The direction $[rst]_{agg}$ is drawn here normal to the plane of the paper. Therefore, $[rst]_{agg}$ and $[uvw]_{sub}$ are parallel.

This suggests considerable flexibility in the use of these materials as LDE substrates for nucleation of organic materials.[28]

The LDE concepts described above suggest that this mechanism can be exploited to design substrates for selective nucleation of polymorphs. Polymorphs of a given composition are described by different supramolecular motifs in the solid state. Therefore, crystal planes of different polymorphs differ with respect to their two-dimensional molecular structures and dihedral angles, which correspond to θ_{agg}. If a particular polymorph of a compound has two well-defined, close-packed crystal planes whose dihedral angle matches that of the substrate ledge site, nucleation of that phase will be favored. Conversely, nucleation of a polymorph which lacks a pair of intersecting close-packed planes, or which has intersecting close-packed planes whose dihedral angle is not equal to θ_{sub}, will be less preferred.

Results and Discussion

The $DMTC^+-TMO^-$ salts crystallize into numerous polymorphic forms which can be readily distinguished by their colors and morphologies and, for some phases, by their X-ray powder diffraction patterns. It was previously reported that as many as seven forms of $DMTC^+-TMO^-$ salts crystallized by slow evaporation of $CHCl_3$ solutions, although only two forms were obtained in sufficient quantity and quality for single-crystal X-ray analysis. These two forms both crystallize as rectangular plates and were designated **Ia** and **Ib** (**Ia**: space group $P2_1/c$, $a = 7.660$ Å, $b = 23.950$ Å, $c = 20.201$ Å, $\beta = 82.35°$; **Ib**: space group $P2_1/a$, $a = 14.528$ Å, $b = 13.676$ Å, $c = 18.548$ Å, $\beta = 90.54°$).[22] These two polymorphs are readily distinguished by their color, with **Ia** exhibiting a red color by transmission but a gold color by reflection and **Ib** exhibiting a red color by both transmission and reflection. The two phases can be identified by their visible absorption spectra, with **Ia** exhibiting peaks with λ_{max} values of 510 and 610 nm and **Ib** exhibiting peaks with λ_{max} values of 490, 570 (shoulder), and 600 nm.[29] We have verified the simultaneous formation of these phases during evaporation of $CHCl_3$ solutions, although **Ia** was *always* the dominant phase. We have also observed significant amounts of a purple phase, designated as **Ic** in ref 22. Polymorph **Ib** was clearly the minor phase in all attempts using conventional crystallization procedures.

Inspection of the X-ray single crystal structure of **Ia**,**b** reveals dramatic differences in packing motifs. In both structures, the $DMTC^+$ and TMO^- ions stack in an alternating manner along the *b* axis, but in **Ia**, the ions are mutually perpendicular, while in **Ib** they are mutually parallel (Figure 2). This difference in solid-state packing leads to unique packing densities in the various crystal planes. In **Ia**, $DMTC^+$ and TMO^- ions form $(10\bar{1})_{Ia}$ layers which can be described as a close-packed, low-energy plane. All other planes exhibit a significant degree of molecular corrugation; that is, formation of close-packed surfaces from these planes would require cleaving bonds in molecules. In contrast, **Ib** has two planes with close-packed surfaces, namely $(010)_{Ib}$ and $(001)_{Ib}$. Further inspection of the crystal structure of **Ib** also reveals a $(014)_{Ib}$ plane which can be generated by removal of a $CHCl_3$ solvate molecule. This plane can be considered as locally close-packed when viewed as an aggregate consisting of $DMTC^+-TMO^-$ ion pairs stacked along the *a* axis. This aggregate, which is outlined in Figure 2, is important for the discussion below.

Crystallization of $DMTC^+-TMO^-$ salts from $CHCl_3$ solu-

(28) Crystallographic ledge dihedral angles, θ_{sub}, for diacids with the general formula $HOOC(CH_2)_nCOOH$) given as (*n*, ledge direction, θsub): (2, [101], 112.6°); (3, [001], 123.4°); (4, [100], 126.7°); (5, [001], 90.0°, 128.5°, 141.4°); (6, [101], 125.2°); (7, [101], 122.7°); (8, [100], 124.3°); (9, [001], 90.0°, 129.4°, 140.7°); (10, [101], 123.2°); (11, [001], 90.0°, 129.7°, 140.3°). Multiple possibilities for ledge dihedral angles are given for compounds exhibiting multiple combinations of close-packed planes sharing a common ledge direction.

(29) The absorptions at 510 nm for **Ia** and 490 nm for **Ib** were slightly different that the values of 500 and 510 nm, respectively, estimated from the UV−vis spectra reported in ref 22. The values reported here were observed consistently for these phases.

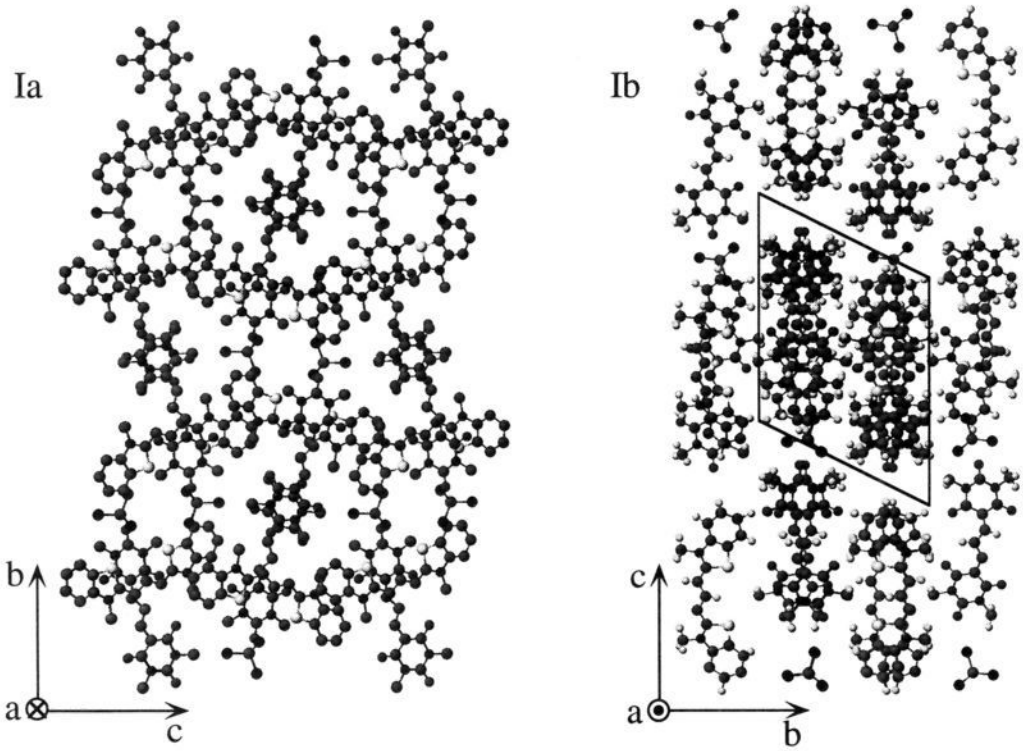

Figure 2. Solid-state packing of polymorphs **Ia**,**b** as viewed normal to their (100) planes. The rather complex motif of **Ia**, in which $DMTC^+$ and TMO^- ions are mutually perpendicular, reveals that only the $(10\bar{1})_{Ia}$ plane can be considered close-packed. In contrast, the $(010)_{Ib}$ and $(001)_{Ib}$ planes of **Ib** are close-packed. A small aggregate of **Ib**, indicated by the outlined region, has a $(014)_{Ib}$ plane which can be considered close-packed over the length scale of a unit cell. This plane would result if the $CHCl_3$ solvate molecule is removed from the $(001)_{Ib}$ plane.

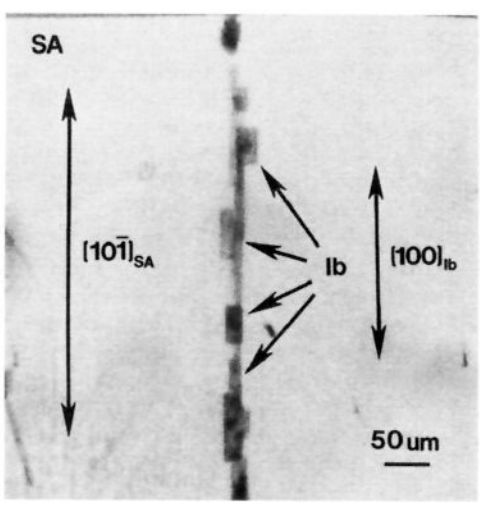

Figure 3. Photograph of crystals of the red polymorph **Ib** grown at a $[10\bar{1}]_{SA}$ ledge from $CHCl_3$ solutions containing 7.5×10^{-5} M DMTC and TMO. The $[10\bar{1}]_{SA}$ ledge is oriented vertically.

tions in the presence of freshly cleaved SA crystals afforded a dramatically different polymorph distribution than that observed in the absence of SA. After approximately 24 h, highly oriented red crystals were evident on the $[10\bar{1}]_{SA}$ ledges (Figure 3). These crystals were flat, rectangular plates with dimensions of approximately 50×15 μm and with their long axes parallel to the $[10\bar{1}]_{SA}$ ledge. Under the conditions employed crystallization occurred exclusively on the ledge sites.[30]

The crystals grown on the SA substrate ledges were red by transmitted light and did not exhibit a gold color by reflection, consistent with the formation of polymorph **Ib**. This assignment was supported by UV−vis spectroscopy of these crystals, which exhibited the same features as bulk **Ib**.[29] Upon heating, crystals attached to SA ledges fractured and changed shape and orientation at 100 °C. This behavior is consistent with stress-induced jumping and bending reported previously for crystals of **Ib** at this temperature.[22] In contrast, **Ia** does not exhibit thermally induced mechanical stresses. Selective nucleation and growth of **Ib** was also achieved in "batch mode" crystallization experiments performed in the presence of freshly ground microscopic seeds of SA suspended in $CHCl_3$. Slow evaporation of the SA/$CHCl_3$ suspensions containing 7.5×10^{-5} M DMTC and TMO to near dryness resulted in the formation of red microcrystals of **Ib**. In contrast, **Ia**,**c** were the primary phases observed in the absence of the SA microcrystals. On the basis of the observation that $[10\bar{1}]_{SA}$ ledges are formed when SA single crystals are cleaved, the shear stress during grinding of the microcrystals is expected to produce these ledges, which then can induce the nucleation of **Ib** in the same manner as the large single crystals.

The small size of the **Ib** crystals grown at the $[10\bar{1}]_{SA}$ ledge prevented an orientation assignment by standard X-ray diffraction methods or by optical goniometry. However, previous reports demonstrated that atomic force microscopy (AFM) can be used to index crystals as small as 1 μm by obtaining molecularly resolved surface structure and the corresponding lattice parameters of crystal faces, by characterization of surface topography, and by "AFM goniometry".[31] AFM images of the large, exposed face of **Ib** crystals attached to the SA ledges revealed ledges on the **Ib** crystals which were parallel to the substrate $[10\bar{1}]_{SA}$ ledge (not shown). On the basis of the crystal

(30) Occasionally, randomly oriented crystals were observed in surface pits on dried SA substrates. Our experience suggests that this was due to evaporation of nutrient-rich $CHCl_3$ trapped in these defects upon removal of the substrate crystals from solution. These crystals were too small and their amounts too minor for characterization.

(31) Hillier, A.; Ward, M. D. *Science* **1994**, *268*, 1261.

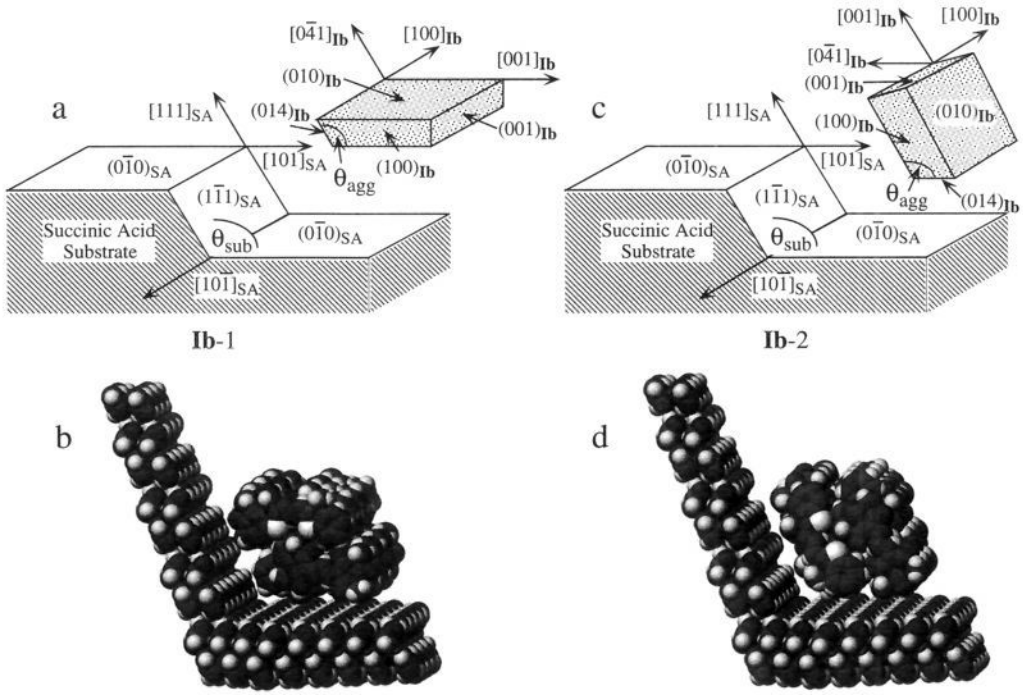

Figure 4. (a) Schematic representation of orientation **Ib**-1 at the $[10\bar{1}]_{SA}$ ledge. In this orientation, the $(010)_{Ib}$ and $(014)_{Ib}$ planes are in contact with $(0\bar{1}0)_{SA}$ and $(1\bar{1}1)_{SA}$, respectively, and $[100]_{Ib}$ is parallel to the $[10\bar{1}]_{SA}$ ledge. The value of $\theta_{agg} = 113.0°$ for $(014)_{Ib} \cap (010)_{Ib}$ is nearly identical to $\theta_{sub} = 112.6°$ for the $[10\bar{1}]_{SA}$ ledge. (b) Space-filling model of a **Ib** prenucleation aggregate in orientation **Ib**-1 in proximity to the $[10\bar{1}]_{sa}$ ledge. (c) Schematic representation of orientation **Ib**-2 at the $[10\bar{1}]_{SA}$ ledge. In this orientation, the $(010)_{Ib}$ and $(014)_{Ib}$ planes are in contact with $(1\bar{1}1)_{SA}$ and $(0\bar{1}0)_{SA}$, respectively. Note that this is reversed from orientation **Ib**-1. The $[100]_{Ib}$ direction remains parallel to the $[10\bar{1}]_{SA}$ ledge. The value of $\theta_{agg} = 113.0°$ for $(014)_{Ib} \cap (010)_{Ib}$ is nearly identical to $\theta_{sub} = 112.6°$ for the $[10\bar{1}]_{SA}$ ledge. (d) Space-filling model of a **Ib** prenucleation aggregate in orientation **Ib**-2 in proximity to the $[10\bar{1}]_{SA}$ ledge. The one-dimensional aggregates in b and d both have $[100]_{Ib}$ parallel to the $[10\bar{1}]_{SA}$ ledge and have cross sections identical to the outlined region in Figure 2.

structure of **Ib**, it is reasonable to assign these features as $[100]_{Ib}$ ledges, as these are expected to be reinforced by intermolecular $\pi-\pi$ interactions between the $DMTC^+$ and TMO^- ions along the stacking $[100]_{Ib}$ direction. The correspondence between anisotropic intermolecular bonding and topographical features observed by AFM has been demonstrated previously for one-dimensional stacks in organic conductors.[32] The assignment of these ledges to $[100]_{Ib}$ is consistent with the observation that the long axes of macroscopic **Ib** crystals were parallel to the ledge as previous morphological studies assigned the long **Ib** crystal axis to the $[100]_{Ib}$ direction.[22] This morphology reflects the $\pi-\pi$ interactions between $DMTC^+$ and TMO^- ions that are responsible for the formation of $[100]_{Ib}$ ledges.

The step planes of the $[100]_{Ib}$ ledge could comprise $(010)_{Ib}$ or $(001)_{Ib}$ planes, which are relatively close-packed and therefore would have low surface energies. However, the actual step planes of **Ib** crystals, as well as their terrace planes, depend upon their orientation with respect to the substrate. Orientation **Ib**-1 refers to that in which the $(010)_{Ib}$ plane contacts the $(0\bar{1}0)_{SA}$ terrace, whereas orientation **Ib**-2 corresponds to that in which $(010)_{Ib}$ contacts $(1\bar{1}1)_{SA}$ (Figure 4). Orientations **Ib**-1 and **Ib**-2 should be distinguishable by AFM as the lattice parameters, and the symmetries of the crystal planes facing the AFM tip would differ significantly. In the case of **Ib**-1, the crystal plane facing the AFM tip would be $(010)_{Ib}$ and the step plane would be $(001)_{Ib}$, whereas for **Ib**-2 the converse would exist.

Molecular scale AFM images of the upper crystal face obtained in air reveal ordered regions (Figure 5). While some disorder is evident,[33] the Fourier transform of the AFM data indicate strong components at angles of 49° and 144° from the horizontal axis of the image, corresponding to d spacings of 6.5 and 5.1 Å, respectively. Comparison of the Fourier transform with the crystal structure of **Ib** reveals that the strong components are consistent with the spacings between slightly contracted $(201)_{Ib}$ ($d = 6.74$ Å) and $(10\bar{3})_{Ib}$ ($d = 5.71$ Å) planes, which are parallel and normal to the molecular planes, respectively.[34] The dihedral angle between these planes is 92°, nearly identical to the 95° angle between Fourier components. The $(201)_{Ib}$ and $(10\bar{3})_{Ib}$ planes are perpendicular to $(010)_{Ib}$. Therefore, the AFM data are consistent with orientation **Ib**-1, that is, with $(010)_{Ib}$ facing the AFM tip. This orientation also is consistent with the step heights on the **Ib** crystals, which ranged from 15 to 21 Å, corresponding to two or three $(010)_{Ib}$ molecular layers. Furthermore, the symmetry and intensities of the Fourier transform components exhibit 2-fold and inversion symmetry in the imaged crystal plane but an *absence* of mirror symmetry. The monoclinic $P2_1/a$ lattice has a 2-fold rotation axis parallel to b and a mirror plane perpendicular to b. Therefore, the

(32) Hillier, A.; Carter, P. W.; Ward, M. D. *J. Am. Chem. Soc.* **1994**, *116*, 944.

(33) The disorder in the AFM data is not completely understood, but it is likely due either to compliance of the sample under the force of the AFM tip or to loss of $CHCl_3$ solvate molecules from the surface. The latter may result in voids with concomitant surface reconstruction and disorder.

(34) The tendency for contraction along the direction normal to $(201)_{Ib}$ is expected to be minimal, as the close-packing and $\pi-\pi$ interactions between $DMTC^+$ and TMO^- ions along this direction are not likely to be perturbed significantly by the loss of solvent. Conversely, the contraction of $DMTC^+$ and TMO^- ions along the direction normal to $(10\bar{3})_{Ib}$ to compensate for these voids and loss of hydrogen bonding (to $CHCl_3$) is more likely. These qualitative differences may account for the experimentally observed large contraction of the $(10\bar{3})_{Ib}$ d spacing (−10.7%) and only a slight contraction of the $(201)_{Ib}$ d spacing (−3.7%), compared to the values expected on the basis of single-crystal X-ray diffraction. We note that the latter is within the error of the AFM measurement.

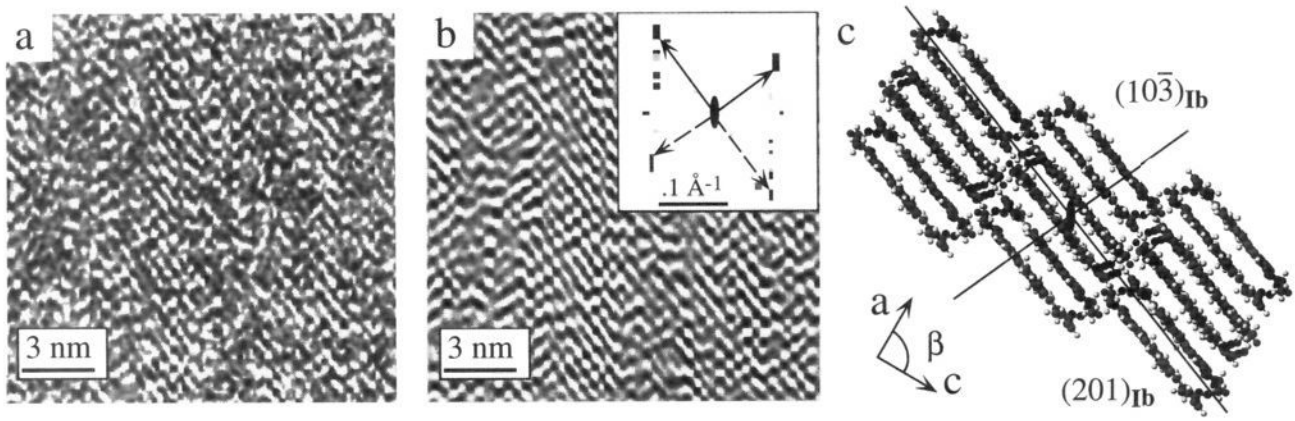

Figure 5. (a) Atomic force microscopy data of **Ib** crystals grown at the $[10\bar{1}]_{SA}$ ledge (low-pass filtered). (b) Fourier filtered atomic force microscopy data from a. The Fourier transform of the real space data (inset) reveals 2-fold symmetry normal to the imaged plane, indicated by the solid oval symbol, but the absence of mirror symmetry. Vectors are drawn to the strongest components as a visual aid. (c) View of the molecular packing of the $(010)_{Ib}$ plane depicting the $(201)_{Ib}$ and $(10\bar{3})_{Ib}$ planes. The 2-fold rotation axis normal to $(010)_{Ib}$ is indicated by the solid oval symbol.

Fourier transform unambiguously establishes orientation **Ib**-1 with $(010)_{Ib}$ facing the AFM tip and in contact with the $(0\bar{1}0)_{SA}$ terrace. The contrast in the real AFM data also resembles the molecular motif of the $(010)_{Ib}$ plane. In contrast, the real and Fourier data lack any correlation to the structure of the $(001)_{Ib}$ plane.

Comparison of the crystal packing of **Ia** and **Ib**, and its relationship to the geometry of the $[10\bar{1}]_{SA}$ ledge site, reveals a plausible explanation, based on LDE, for the selectivity toward **Ib**. The solid-state structure of **Ia** reveals only one plane with a close-packed surface, namely $(10\bar{1})_{Ia}$ and no reasonable crystal plane combinations with a dihedral angle approaching that of the $[10\bar{1}]_{SA}$ ledge. Therefore, strong interfacial interaction between a prenucleation aggregate of **Ia** with both planes of the $[10\bar{1}]_{SA}$ ledge is not possible, consistent with the absence of growth of this polymorph in the presence of SA.

Polymorph **Ib** has close-packed $(001)_{Ib}$ and $(010)_{Ib}$ planes, but the dihedral angle between these planes corresponds to $\theta_{agg} = 90°$. While this would appear to disqualify the nucleation of **Ib** by LDE at the $[10\bar{1}]_{SA}$ ledge, analysis of the crystal structure of **Ib** reveals the existence of an aggregate within the unit cell having locally close-packed $(010)_{Ib}$ and $(014)_{Ib}$ planes (the $(014)_{Ib}$ plane can be generated by removal of a $CHCl_3$ solvate molecule from the $(001)_{Ib}$ plane; see outline, Figure 2). The dihedral angle of $(010)_{Ib} \cap (014)_{Ib}$ corresponds to $\theta_{agg} = 113.0°$, nearly identical to the value of $\theta_{sub} = 112.6°$ for the $[10\bar{1}]_{SA}$ ledge. This affords a dihedral angle mismatch of 0.4%.[35] The $(010)_{Ib}$ and $(014)_{Ib}$ planes share the $[100]_{Ib}$ direction; therefore $[100]_{Ib}$ would coincide with $[10\bar{1}]_{SA}$ if these aggregate planes contact the SA ledge planes (Figure 4). This is consistent with the orientation which was assigned on the basis of the morphology and AFM of **Ib** single crystals grown at the SA ledges. This orientation results in a one-dimensional lattice mismatch of 4.7% along the ledge,[36] which is within values observed in previous examples of LDE systems.[21]

Both orientations **Ib**-1 and **Ib**-2 preserve the match between the aggregate and ledge dihedral angles *and* the orientation of $[100]_{Ib}$ along $[10\bar{1}]_{SA}$. Evidently, there is a greater free energy lowering for **Ib**-1 (*vide infra*). In both cases sustained interfacial contact between $(014)_{Ib}$ and the SA substrate as the crystal grows

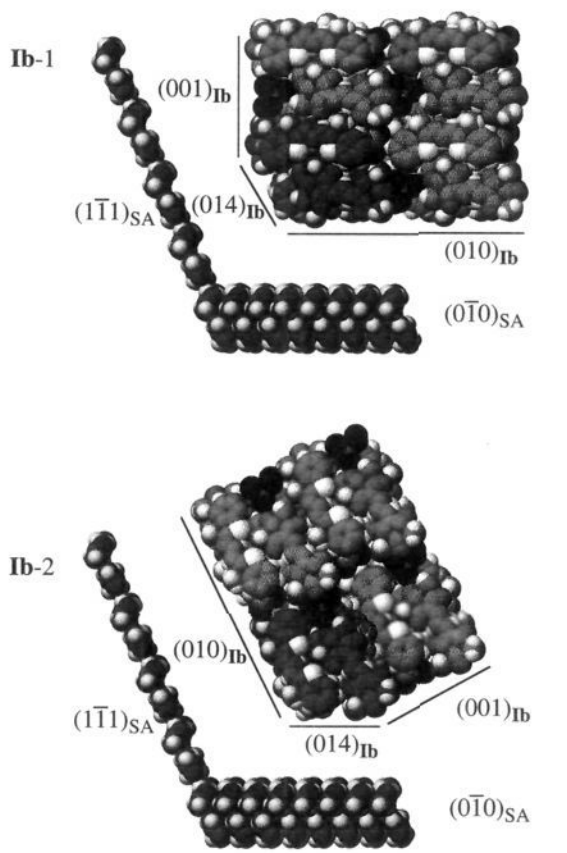

Figure 6. Schematic representation of **Ib** at the $[10\bar{1}]_{SA}$ ledge after growth from the prenucleation aggregate depicted in Figure 4, for orientation **Ib**-1 and orientation **Ib**-2. The view is normal to the $[10\bar{1}]_{SA}$ ledge direction, which is coincident with the hydrogen-bonded chains. The $(010)_{Ib}$ plane of orientation **Ib**-1 maintains interfacial contact with the $(0\bar{1}0)_{SA}$ terrace throughout the growth process, but the close-packed $(001)_{Ib}$ plane diverges from the $(1\bar{1}1)_{SA}$ step. In contrast, the $(010)_{Ib}$ plane of orientation **Ib**-2 maintains contact with the $(1\bar{1}1)_{SA}$ step in the growth process. In both cases, the critical interaction in the initial stages of LDE involves the close-packed $(014)_{Ib}$ and $(010)_{Ib}$ planes of the aggregate, which is darkened relative to the rest of the molecules in the nuclei. The divergence of one plane of **Ib** from the substrate in either orientation argues for one-dimensional aggregation along the ledge in the initial stages of nucleation, that is growth along $[100]_{Ib}$ (see Scheme 1).

(35) The dihedral angle mismatch was calculated according to the following equation: % mismatch = (|(lattice constant)$_{Ib}$ − (lattice constant)$_{SA}$|/(lattice constant)$_{SA}$) × 100.

(36) In this case the mismatch was calculated by comparing reasonable integral multiples of the lattice constants: $2 \times |[10\bar{1}]_{SA}| = 2 \times 7.62$ Å = 15.24 Å; $|[100]_{Ib}| = 14.528$ Å. Using these two lattice constants and the formula in ref 35 gives a value of 4.7%.

Scheme 1

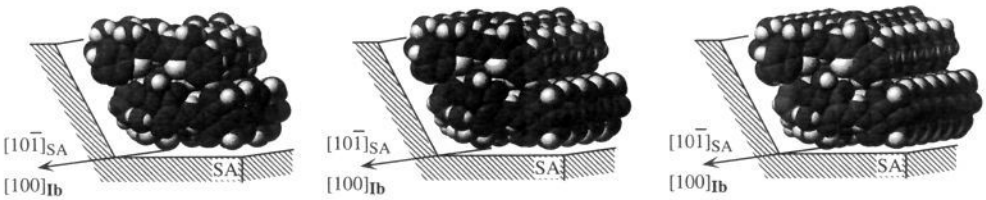

in directions normal to the $[10\bar{1}]_{SA}$ ledge is not possible for either orientation because the $(014)_{Ib}$ plane actually cuts through $DMTC^+$ and TMO^- ions in the bulk structure (Figure 6). In the case of **Ib**-1, the morphologically important close-packed $(001)_{Ib}$ plane diverges from the $(1\bar{1}1)_{SA}$ step. This argues that interfacial free energy lowering of the aggregate stems from LDE-driven nucleation involving growth of a one-dimensional aggregate *along the ledge* until the nucleus reaches critical size. The interfacial contact at the ledge and $\pi-\pi$ stacking interactions between $DMTC^+$ and TMO^- ions along $[001]_{Ib}$ favor rapid growth of the aggregate along the ledge direction in the initial stages (Scheme 1 illustrates the stepwise growth of a one-dimensional aggregate along the ledge corresponding to a length of 4, 8, and 12 ion pairs, for a total of 8, 16, and 24 ion pairs in the aggregate). This process involves the $(014)_{Ib}$ and $(010)_{Ib}$ planes of a one-dimensional aggregate whose cross section corresponds to the area outlined in Figure 2. Aggregate assembly in this manner preserves the dihedral angle match and close-packed planes at the ledge interface, thereby maximizing dispersive contact during nucleation. Once the nucleus has reached critical size, the orientation of **Ib** is established and growth can occur from these nuclei without need for further stabilization by the $(1\bar{1}1)_{SA}$ step. It is important to note that the height of the **Ib** crystals far exceeds that of the ledge height. Therefore, the macroscopic morphology of **Ib** crystals will be determined ultimately by the bulk crystal intermolecular interactions and surface energies.

Nucleation by growth of an aggregate primarily along the ledge is a reasonable description of LDE events as free energy lowering of the nuclei by interaction with both planes of the substrate ledge will favor the growth of one-dimensional nuclei with small critical sizes (<10 nm, involving only tens of molecules).[21] These estimates were conservative, as only interfacial dispersive LDE interactions were considered and the volume free energy of the aggregate was ignored. However, these calculations only pertained to nucleation in the gas phase, that is, in the absence of solvent. The strength of dispersive forces between two entities are substantially reduced in the presence of a solvent, the extent of this reduction determined by the dielectric properties of the different phases.[37] The magnitude of the interfacial interaction energy in the presence of solvent can be deduced from calculation of the nonretarded Hamaker constant (A) according to a modified version of Lifshitz theory,[38,39] where A represents the magnitude of the van der Waals energy. In the case of $CHCl_3$, the dispersive attraction between two identical species is reduced by roughly a factor of 30 compared to the interaction in free space. The interaction between two dissimilar components across a solvent medium is still favorable provided the refractive index of the solvent medium is *not* intermediate between the refractive indices of two dissimilar species (if this condition is not met, the dispersion force can actually be repulsive). Given the refractive indices for SA ($n_1 = 1.534$),[40] **Ib** ($n_2 \approx 1.7$),[41] and $CHCl_3$ ($n_3 = 1.45$),[42] the dispersive interactions between SA and **Ib** are attractive. These calculations indicate that $A \approx 6.4 \times 10^{-21}$ J for this interaction. While this value is nearly 20 times smaller than the value in free space calculated in the same manner, the positive value of A indicates that the van der Waals interactions remain favorable. The smaller value of A in $CHCl_3$ suggests that the critical size may be somewhat larger in this solvent compared to free space.

We previously modeled the growth of the prenucleation aggregate on a single-crystal substrate ledge as a cylinder interacting with the ledge planes.[21] The interaction energy, $W(D)$, for this geometry is given by eq 8, where A is the

(37) The van der Waals free energy between two identical molecules in a solvent medium is given by

$$w(r) = -\left[3kT\left(\frac{\epsilon_1(0) - \epsilon_3(0)}{\epsilon_1(0) + 2\epsilon_3(0)}\right)^2 + \frac{\sqrt{3}h\nu_e}{4}\frac{(n_1^2 - n_3^2)^2}{(n_1^2 + 2n_3^2)^{3/2}}\right]\frac{a_1^6}{r^6}$$

where ϵ_1 and n_1 and ϵ_3 and n_3 are the dielectric constants and refractive indices of the molecule and the solvent medium, respectively, a_1 is the radius of the molecule (assumed to be spherical), ν_e is the dipole oscillation frequency, and r is the distance between molecules. If the first term of the equation, which describes the zero-frequency dipolar contribution is ignored (the SA substrate has no dipole in the ledge planes), the reduction in the interaction energy due to the solvent can be estimated from the second term, which describes the dispersive interactions. Furthermore, the dispersive contribution is usually greater as $h\nu_e \gg kT$ under most conditions. The reduction in dispersive energy upon replacing free space ($\epsilon = 1$) by $CHCl_3$ therefore can be estimated from

$$\frac{[(n_1^2 - n_3^2)^2(n_1^2 + 2n_3^2)^{-3/2}]_{\text{free space}}}{[(n_1^2 - n_3^2)^2(n_1^2 + 2n_3^2)^{-3/2}]_{CHCl_3}}$$

which, based on the known values for a typical organic ($n_1 = 1.5$) and for $CHCl_3$ ($n_3 = 1.45$), give a reduction in dispersive energy of approximately 30. It should be noted that, while the interaction energy for a molecule approaching a *surface* actually scales as r^{-3}, the influence of the solvent medium remains.

(38) Israelachvilli, J. *Intermolecular and Surface Forces*; Academic Press: New York, 1992.

(39) The Hamaker constant (A) refers to the term describing the magnitude of the van der Waals energy, which scales (in the absence of retarding forces) according to $w(r) = -Ar^{-6}$. A positive value of A therefore signifies an attractive van der Waals energy. According to a modified form of the Lifshitz theory, the Hamaker constant can be expressed as the sum of the zero-frequency dipolar contribution and the dispersive contribution

$$A \approx \frac{3}{4}kT\left(\frac{\epsilon_1 - \epsilon_3}{\epsilon_1 + 2\epsilon_3}\right)\left(\frac{\epsilon_2 - \epsilon_3}{\epsilon_2 + 2\epsilon_3}\right) + \frac{3h\nu_e}{8\sqrt{2}}\frac{(n_1^2 - n_3^2)(n_2^2 - n_3^2)}{(n_1^2 + n_3^2)^{1/2}(n_2^2 + n_3^2)^{1/2}[(n_1^2 + n_3^2)^{1/2} + (n_2^2 + n_3^2)^{1/2}]}$$

where $\epsilon_1 = 2.35$, $\epsilon_2 \approx 3$, and $\epsilon_3 = 4.81$. The values of ϵ_1 and ϵ_2 were obtained by assuming the approximation $\epsilon \approx n^2$. For SA|$CHCl_3$|**Ib**, $A \approx 6 \times 10^{-21}$ J; whereas for SA|free space|**Ib**, $A \approx 10 \times 10^{-20}$ J. This latter value is comparable to those calculated for other organic nucleants on the SA substrate.[21]

(40) Winchell, A. N. *The Optical Properties of Organic Compounds*; Academic Press Inc.: New York, 1954; p 33.

(41) The refractive index of **Ib** is unknown. The n_2 value used here was chosen on the basis of values of organic compounds with charge-transfer functionalities (see ref 40). While a larger refractive index may be expected for an organic dye, the charged nature of the dye would be expected to diminish the polarizability and, therefore, the magnitude of n_2 (according to the Lorenz−Lorentz equation). Calculations indicate that the Hamaker constant A increases with increasing n_2, Therefore, the value of A calculated here on the basis of $n_2 = 1.7$ represents a conservative estimate of the SA−**Ib** interaction across $CHCl_3$.

(42) *Handbook of Chemistry and Physics*; Weast, R. C., Astle, M. J., Eds.; CRC Press, West Palm Beach, FL, 1978.

$$W(D) = -(ALR^{0.5})/(17D^{1.5}) \quad (8)$$

Hamaker constant, L is the length of an aggregate stack, R is the effective radius of the aggregate cylinder, and D is the contact distance between the aggregate and the substrate. It is important to note that the Hamaker constant is more accurately described by including all the terms of the van der Waals coefficient, C_{vdw}, which is the sum of Debye induction (C_{ind}), Keesom orientation (C_{orient}), and dispersion (C_{disp}) terms.[43] The first two terms would include dipolar interactions due to ($DMTC^+$)(TMO^-) ion pairs, whose dipoles (approximately 14 D if point charges separated by 3.5 Å are assumed) will be oriented along the SA ledge. The growth of **Ib** at the $[10\bar{1}]_{SA}$ ledge will not be influenced by C_{orient} because the dipoles are not freely rotating as required by the Keesom limit. Contribution from C_{orient} assuming *fixed* dipole−dipole interactions also is negligible due to the absence of a dipole in SA along the $[10\bar{1}]_{SA}$ ledge direction. However, it is worthwhile to consider C_{ind} for fixed orientations, which would involve the polarization of an SA molecule in the ledge by the ($DMTC^+$)(TMO^-) dipole. The observed orientation of **Ib** crystals, with the ($DMTC^+$)(TMO^-) dipole parallel to polarizable SA molecules in the $(1\bar{1}1)_{SA}$ step plane, would lead to *weaker* interaction during nucleation between the ($DMTC^+$)(TMO^-) dipole and polarizable SA molecules in the $(1\bar{1}1)_{SA}$ step plane than for other dipole alignments. This argues that dispersive interactions govern the nucleation of **Ib** at the SA ledges. Furthermore, the longer range $D^{-1.5}$ dependence in eq 8, which contrasts with the r^{-6} dependence for van der Waals interaction between two molecules, stems from the requirement that the interaction energy be integrated *over the entire volume of the substrate and the cylinder*. Given the centrosymmetric nature of the substrate and **Ib**, including aggregates of the latter that exceed the unit cell dimensions, it seems reasonable the C_{ind} would not dominate the LDE. The nondirectional nature of dispersive interactions results in a growth orientation which is dictated by the well-defined topography of the crystal and a geometric match between the substrate ledge and prenucleation aggregate.

The observation of highly oriented growth in spite of a 4.7% lattice mismatch between $[100]_{Ib}$ and $[10\bar{1}]_{SA}$ is consistent with dispersive interactions governing the nucleation process. On the basis of previous studies of dispersive interfaces, poor commensurism can be tolerated as these interfaces have substantial interface compressibilities (or equivalently, small interfacial moduli). This condition, which for two-dimensional interfaces has been described as "quasiepitaxy",[44] leads to small stresses along the lattice vectors even though commensurism only exists if multiples of the matching vectors are considered. A simple analysis of the SA-**Ib** interfaces suggests that one-dimensional quasiepitaxy may play a role in the preferential nucleation of **Ib**-1 over **Ib**-2. If the directions contained in *contacting* interfaces which are normal to the ledge direction are considered (see Figures 1 and 4), the relevant matching lattice vectors are $[001]_{Ib}$:$[101]_{SA}$ for **Ib**-1 and $[001]_{Ib}$:$[111]_{SA}$ for **Ib**-2. The overall length of a lattice vector used to calculate mismatch can then be expressed as $n|uvw|$, where n is the integral number of repeats of a lattice vector with a magnitude $|uvw|$. Using this format, smaller lattice mismatches can be found for **Ib**-1 (0.13% for $2|[001]_{Ib}|$:$5|[101]_{SA}|$) than for **Ib**-2 (3.4% for $1|[001]_{Ib}|$:$2|[111]_{SA}|$ in **Ib**-2).[45] Favorable interfacial interaction resulting from the quasiepitaxy between the close-packed $(010)_{Ib}$ and $(0\bar{1}0)_{SA}$ planes during growth from the aggregate in orientation **Ib**-1 may be responsible for the large widths of the crystals as compared to their heights.

Conclusion

We have demonstrated that selective growth of a less preferred polymorph can be achieved through ledge-directed epitaxy. This requires careful choice of a substrate whose ledge geometry matches that of a prenucleation aggregate corresponding to that polymorph. The critical factors are similar dihedral angles for the ledge and aggregate planes, interface planes which are close-packed, and attractive dispersive interactions. The unique relationship between the ledge and aggregate geometry also governs the orientation of the growing crystals, which in turn can be used to deduce the nature of the epitaxial interactions. Although interplanar epitaxy may play a secondary role in the azimuthal orientation of observed polymorph, it is clear that the primary events are driven by LDE. The availability of other alkanoic diacid crystals in which one-dimensional hydrogen bonding reinforces ledge sites with different ledge angles suggests a library of substrates specific for polymorphs of other organic compounds. Furthermore, it is likely that the choice of substrates can be extended to other crystalline solids that have one-dimensional anisotropy, such as para-substituted aromatic diacids and low-dimensional charge-transfer solids. It is anticipated that extension of these principles to other polymorphic systems, including other dye crystals and pharmaceutics, can lead to effective control of crystal growth processes.

Acknowledgment. The authors acknowledge the National Science Foundation for financial support and the Office of Naval Research for an equipment grant.

JA951020H

(43) For dissimilar molecules, $C_{vdw} = C_{disp} + C_{orient} + C_{ind}$. When the molecules are in a fixed orientation

$$C_{disp} = \frac{[1.5\alpha_{01}\alpha_{02}I_1I_2]}{(I_1 + I_2)(4\pi\epsilon_0)^2};$$

$$C_{orient} = \mu_1\mu_2\frac{[2\cos\theta_1\cos\theta_2 - \sin\theta_1\sin\theta_2\cos\phi]}{4\pi\epsilon_0 r^3};$$

$$C_{ind} = \frac{\mu_1^2\alpha_{02}(1 + 3\cos^2\theta)}{2(4\pi\epsilon_0)^2}$$

where the subscripts 1 and 2 designate the aggregate and substrate, μ is the experimental dipole moment, α_0 is the calculated molecular polarizability, I is the experimental ionization potential, θ is the angle between a dipole axis and an axis connecting the aggregate and substrate, and ϕ is the dihedral angle between aggregate and substrate dipoles.[21]

(44) Forrest, S. R.; Zhang, Y. *Phys. Rev. B* **1994**, *49*, 11297.

(45) Lattice mismatches were calculated according to the following equation % mismatch = (|(lattice constant)$_{Ib}$ − (lattice constant)$_{SA}$|/(lattice constant)$_{SA}$) × 100. The fundamental lattice constants for the interfacial directions are $|[101]_{SA}| = 7.41$ Å, $|[111]_{SA}| = 9.60$ Å, $|[0\bar{4}1]_{Ib}| = 14.44$ Å, and $|[001]_{Ib}| = 18.548$ Å.